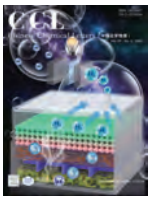
Chinese Chemical Letters 37 (2026) 111172

Contents lists available at ScienceDirect

Chinese Chemical Letters

journal homepage: www.elsevier.com/locate/cclet



An erucin-anchored polymer with excellent amyloidosis inhibition and direct cell membrane penetration ability for intracellular protein delivery

Le Chen [a], Hui Wang [a,*], Yiyun Cheng [b,*]

[a] South China Advanced Institute for Soft Matter Science and Technology, School of Emergent Soft Matter, South China University of Technology, Guangzhou 510640, China

[b] Shanghai Frontiers Science Center of Genome Editing and Cell Therapy, Shanghai Key Laboratory of Regulatory Biology, School of Life Sciences, East China Normal University, Shanghai 200241, China

ARTICLE INFO

Article history:
Received 26 January 2025
Revised 29 March 2025
Accepted 1 April 2025
Available online 2 April 2025

Keywords:
Alzheimer's disease
Aβ aggregation
Protein delivery
Rapid translocation
Oxidative stress

ABSTRACT

Alzheimer's disease (AD) is a complex and multifactorial neurodegenerative disorder, marked by a variety of pathological hallmarks such as oxidative stress (OS), metal accumulation, and the aggregation of amyloid-beta (Aβ) proteins. Erucin, a natural compound present in cruciferous plants, has demonstrated promising therapeutic potential in modulating neurodegenerative diseases, hinting at its neuroprotective capabilities. In this study, we engineered an innovative intracellular protein delivery system centered around erucin. This delivery platform operates through a cell membrane perforation mechanism, enabling the swift translocation of target proteins into the cytoplasm. As a result, it substantially shortens the time required for the proteins to exert their functions. Significantly, this delivery system inherently possesses the capacity to inhibit Aβ aggregation. In PC12 cell models, the delivery of the antioxidant enzyme superoxide dismutase (SOD) successfully mitigated the OS triggered by Aβ aggregation and decreased cytotoxicity. This multifaceted therapeutic strategy holds great promise as an effective approach for the treatment of AD.

© 2026 Published by Elsevier B.V. on behalf of Chinese Chemical Society and Institute of Materia Medica, Chinese Academy of Medical Sciences.

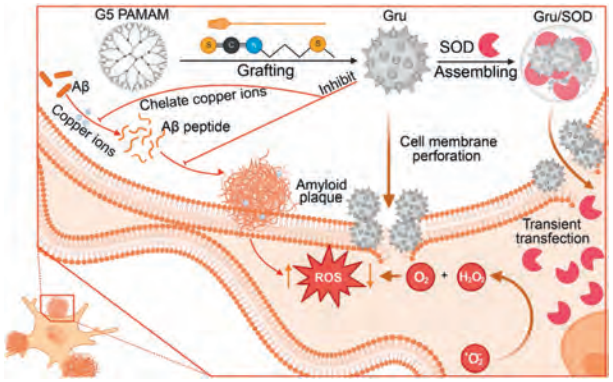
Alzheimer's disease (AD) is the most prevalent neurodegenerative disorder associated with aging, characterized by a complex, multifactorial, and irreversible pathogenesis [1,2]. A hallmark of AD pathology is the formation of β-amyloid plaques, which consist of aggregated amyloid-β (Aβ) peptides [3]. Aβ is neurotoxic in several ways, including inducing pore formation that leads to ion leakage, disruption of cellular calcium homeostasis, and loss of membrane potential [4–7]. It also promotes apoptosis, causes synapse loss, and disrupts the cytoskeleton [8,9]. Current therapeutic approaches for AD primarily aim to slow or halt disease progression, focusing on reducing Aβ production and aggregation or enhancing its clearance [10–13]. However, despite numerous lengthy and expensive clinical trials, no disease-modifying drugs for AD have been approved to date.

Aβ plaques are composed of aggregated Aβ forms combined with metal ions such as copper (Cu^{2+}), iron (Fe^{3+}), or zinc (Zn^{2+}) [13–15]. Both amyloid precursor protein (APP) and Aβ peptides have copper-binding sites, and their interaction with Cu^{2+} can trigger the production of reactive oxygen species (ROS), particularly highly reactive hydroxyl radicals [16,17]. These radicals can induce oxidative damage to Aβ peptides and surrounding molecules (*e.g.*, proteins, lipids), contributing to neurotoxic effects [18]. Thus, there exists a complex and interdependent relationship between Aβ aggregation, oxidative stress (OS), and metal ion imbalance, with each factor significantly influencing the others [19,20]. The multifactorial nature of AD pathology likely explains why current single-target therapies have proven ineffective. Therefore, there is a critical need to develop multifaceted, synergistic treatment strategies to more effectively address this complex disease [21,22].

4-Methylsulfinylbutyl isothiocyanate (Erucin), a bioactive isothiocyanate found in *Eruca sativa* (commonly known as arugula or rocket), a cruciferous vegetable, has shown a range of biological activities, including antioxidant, anti-inflammatory, and neuroprotective effects [23]. Erucin has been shown to inhibit the activation of nuclear factor kappa-light-chain-enhancer of activated B cells (NF-κB), a key regulator of the inflammatory response [23,24]. By suppressing NF-κB activity, erucin reduces the production of pro-

* Corresponding authors.
E-mail addresses: wangh@scut.edu.cn (H. Wang), yycheng@mail.ustc.edu.cn (Y. Cheng).

https://doi.org/10.1016/j.cclet.2025.111172
1001-8417/© 2026 Published by Elsevier B.V. on behalf of Chinese Chemical Society and Institute of Materia Medica, Chinese Academy of Medical Sciences.



Scheme 1. Schematic illustration of erucin-modified dendrimers for Aβ aggregation-inhibition and intracellular antioxidant enzyme delivery in synergistic treatment of Aβ-induced cell death.

inflammatory cytokines such as tumor necrosis factor-α (TNF-α), interleukin-1β (IL-1β), and IL-6, which are typically elevated in AD and contribute to the neuroinflammatory microenvironment. Furthermore, erucin's ability to modulate the release of OS markers, such as malondialdehyde (MDA), further supports its role in mitigating inflammation [25,26]. These properties position erucin as a promising candidate for the development of therapeutic strategies aimed at alleviating the burden of AD.

Given the intricate pathological mechanisms of AD, a single therapeutic approach often proves ineffective. Consequently, we aim to design a multifunctional polymer capable of not only efficiently delivering functional proteins but also exhibiting additional therapeutic effects [27–30]. In this study, erucin was conjugated to a cationic polymer to create a multifunctional polymeric carrier for the intracellular delivery of superoxide dismutase (SOD) as a therapeutic strategy for AD. The erucin-conjugated polymer generates a high number of thiourea and thioether groups, which scavenge ROS, protecting cells from OS and reducing inflammation (Scheme 1).

Polyamidoamine (PAMAM) dendrimers, known for their precise structural design and ease of surface functionalization, have long been recognized as excellent template molecules in drug delivery systems [31,32]. In this study, erucin molecules were directly conjugated with the amino group-terminated G5 PAMAM dendrimer surface to obtain erucin-modified dendrimers. Based on proton nuclear magnetic resonance (^{1}H NMR) analysis (Fig. S1 in Supporting information), the average number of erucin groups grafted onto each dendrimer was determined to be 33, 56, 88, and 105, respectively. The corresponding polymers were named Gru33, Gru56, Gru88, and Gru105, where "G" represents the G5 PAMAM dendrimer, "ru" refers to erucin, and the Arabic numerals denote the number of erucin groups attached to each dendrimer.

We then investigated the intracellular protein delivery efficacies of the polymers in 143B cells using green fluorescence protein green fluorescent protein (GFP) as a model protein [33,34]. As shown in Figs. 1a and b, Gru88 exhibited the highest protein delivery performance, with the fluorescence intensity (FI) of cells treated with Gru88/GFP complexes 11-fold greater than that of the commercial transfection reagent PULSin. An additional increment in the erucin-grafting ratio (Gru105) resulted in diminished efficacy, likely stemming from the equilibrium between erucin modification and the surface cationic charge density (Table S1 and Fig. S2 in Supporting information). Gru88 was then selected as the representative for subsequent independent experiments. The polymer demonstrated good biocompatibility, as neither Gru88 nor the Gru88/GFP complexes caused significant cytotoxicity within the experimental dose range (up to 50 μg/mL) (Fig. S3a in Supporting information).

The optimal dose of Gru88 for GFP delivery in 143B cells was determined to be 25 μg/mL (Fig. S3b in Supporting information),

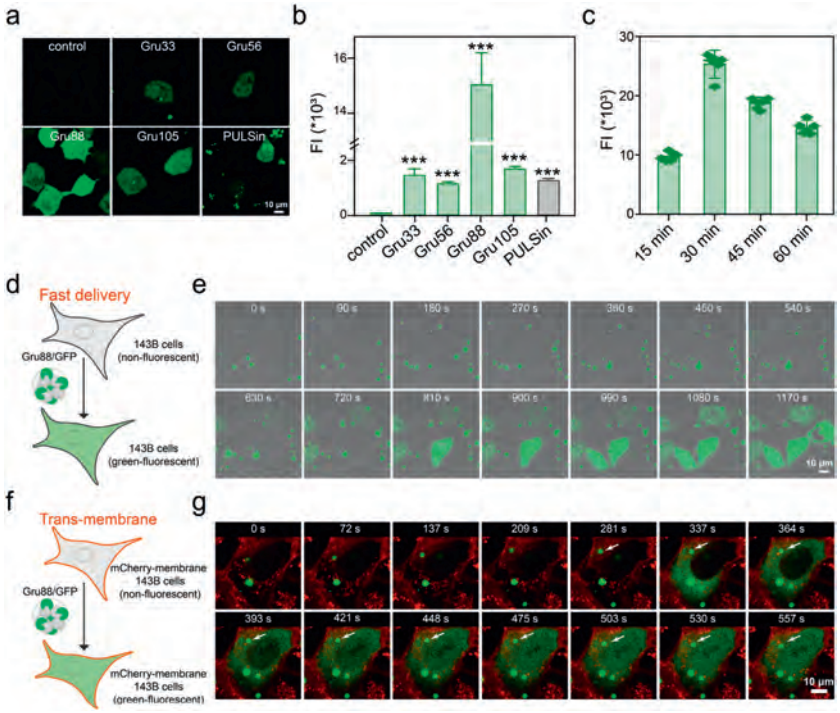


Fig. 1. Gru88 efficiently deliver GFP into 143B cells through a rapid process. Confocal images (a) and FI (b) of 143B cells incubated with Grus/GFP complexes for 0.5 h. (c) Protein delivery efficacy of Gru88 at different incubation times. (d) Schematic illustration of rapid delivery of GFP by Gru88 into 143B cells. (e) Time-slice images of 143B cells incubated with the Gru88/GFP complex. (f) Schematic illustration of transmembrane delivery of GFP by Gru88 into mCherry-membrane-143B cells. (g) Time-slice images of mCherry-membrane-143B cells incubated with the Gru88/GFP complex. The doses of Gru88 and GFP were 25 and 40 μg/mL, respectively. Data are shown as mean ± standard deviation (s.d.) ($n = 3$).

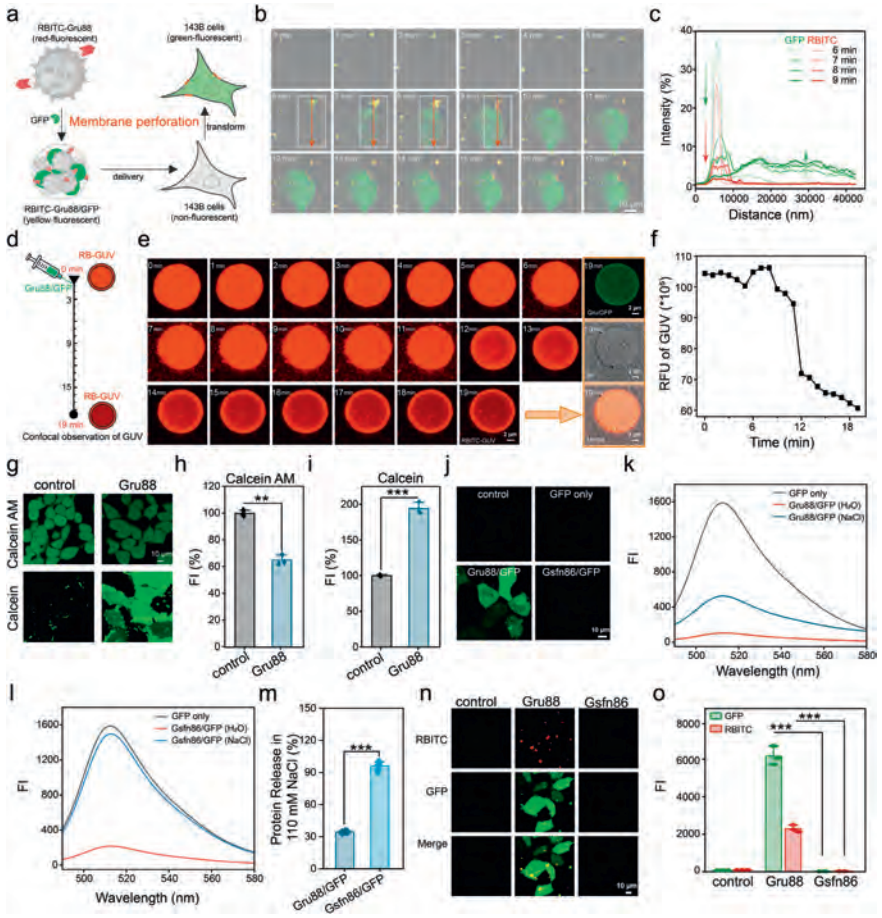


Fig. 2. Gru88 enables intracellular protein delivery through direct membrane perforation. (a) Schematic illustration and (b) time-slice images of 143B cells incubated with the RBITC-Gru88/GFP complex. (c) Statistical analysis of red and green fluorescence intensities along a line at different time points. (d) Schematic illustration of the experimental protocol for GUVs. (e) Confocal images and (f) mean FI of sulforhodamine B-encapsulated GUVs (RB-GUVs). RB-GUVs were incubated with Gru88/GFP complexes and imaged every minute. (g) Confocal images and FI analysis (h-i) of 143B cells treated with calcein AM (h) or calcein (i) after 0.5 h of Gru88 incubation. (j) Confocal images of 143B cells incubated with the Gru88/GFP or Gsfn86/GFP complexes for 0.5 h. FI of the Gru88 (k) or Gsfn86 (l) complexes with GFP in deionized water and NaCl (110 mmol/L) solutions, respectively. (m) Protein release ratio in NaCl (110 mmol/L) solutions determined by k and l. Confocal images (n) and FI (o) of 143B cells incubated with RBITC-Gru88/GFP and RBITC-Gsfn86/GFP complexes for 0.5 h. The polymer and protein concentrations were 25 and 40 μg/mL, respectively. Data are shown as mean ± s.d. ($n = 3$). $^{**}P < 0.01$, $^{***}P < 0.001$.

and the FI of the treated cells peaked 0.5 h after the complex incubation, with a cell positivity rate reaching as high as 85 % (Fig. 1c and Fig. S4 in Supporting information). The rapid diffusion of GFP fluorescence throughout the entire cell in such a short period is intriguing, as traditional nanoparticle endocytosis typically involves membrane bending, changes in surface tension, and the formation of coated pits, processes that usually take several hours to complete [35,36]. To further investigate, we tracked the protein delivery process using a live cell workstation. As shown in Figs. 1d and e, upon adding the Gru88/GFP complexes to the cell culture medium, nanoparticles were observed to accumulate around the cells. After 8 min, uniformly dispersed green fluorescence emerged in some cells. As time elapsed, an increasing number of cells displayed uniformly dispersed green fluorescence. In order to more intuitively observe the process of nanoparticles entering the cell, we carried out the same experiment on 143B cells with a red fluorescently labeled cell membrane (mCherry-membrane-143B). As shown in Figs. 1f and g, the cells immediately exhibited the diffusion of green fluorescence within the cell upon contact between the Gru88/GFP complex particles and the cell membrane (indicated by the white arrow). These results collectively demonstrate that Gru88 can efficiently deliver GFP protein into target cells through a rapid process.

Next, we labeled Gru88 with rhodamine B isothiocyanate (RBITC-Gru88) to track the dynamics of the material within the complex during transmembrane transport. As shown in Figs. 2a and b, upon adding the RBITC-Gru88/GFP complexes to the cell culture medium, yellow clusters appeared around the cells, indicating that the material and protein existed in the form of complexes and accumulated at the cell surface. After 7 min, uniformly dispersed green fluorescence emerged within the incubated cells, suggesting efficient GFP uptake. In contrast, almost no red fluorescence was observed inside the cells throughout the entire experiment, indicating that the material did not enter the cells during GFP delivery (Fig. 2c). The observation that Gru88 does not enter the cell while the protein is rapidly delivered prompts us to hypothesize that the Gru88/protein complex may enter the cells through direct membrane perforation. Giant unilamellar vesicles (GUVs) are spherical lipid bilayer structures that mimicking the structure of natural cell membranes, providing an ideal platform for investigating various aspects of membrane dynamics, including membrane disruption and perforation [37]. In this study, we prepared GUVs encapsulating the membrane-impermeant sulforhodamine B through a natural swelling method (Fig. 2d).

Upon adding the Gru88/GFP complexes to the system, a rapid decrease in the red FI originating from the vesicles was observed

starting from the 8th min (Fig. 2e). This observation indicates membrane disruption and the subsequent release of encapsulated red fluorescence molecules, suggesting a potential alteration in the vesicle membrane integrity. Additionally, after 19 min, a uniform distribution of green fluorescence was detected within the GUVs (Fig. 2f), which further supports the hypothesis that Gru88 facilitates the entry of GFP into the GUVs *via* a membrane disruption mechanism.

We further verified the perforation mechanism of the Gru88 by employing a well-established calcein-acetoxymethylester (calcein-AM) and calcein assay [38]. Calcein-AM is a non-fluorescent, cell-penetrant compound that can be converted into fluorescent but membrane-impermeable calcein through catalysis and hydrolysis by nonspecific esterases within live cells [39,40]. As illustrated in Figs. 2g and h, upon addition of Gru88, the intracellular calcium green AM was released from the cells, resulting in a decrease in intracellular green fluorescence. In a parallel experiment, the extracellular calcium green dye infiltrated the cells, thereby leading to an increase in intracellular green fluorescence (Figs. 2g and i). Collectively, these experimental findings strongly suggest that Gru88 enables the intracellular delivery of GFP through a direct membrane perforation mechanism. We also noticed that Gru88/GFP complexes participate in a conventional endocytosis pathway (Fig. S5 in Supporting information).

Sulforaphane, like erucin, belongs to the class of isothiocyanates. Both sulforaphane and erucin are derived from cruciferous plants and share similar structures, enabling their mutual interconversion [41,42]. The only structural difference between erucin and sulforaphane is the type of sulfur-containing group (methylthio *vs.* methylsulfinyl), leading to slightly different chemical properties and biological activities. In this study, we also synthesized a sulforaphane-conjugated G5 dendrimer to explore the structure-function relationship of erucin in enhancing protein delivery performance. The average number of sulforaphane ligand was 86 (Fig. S6 in Supporting information), and the corresponding polymer was named Gsfn86, where "G" represents the G5 PAMAM dendrimer, "sfn" refers to sulforaphane, and the Arabic numerals denote the number of sulforaphane ligand attached to each dendrimer. As shown in Fig. 2j, while Gru88 efficiently facilitated intracellular delivery of GFP, almost no green fluorescence was observed in 143B cells treated with Gsfn86/GFP complexes. The methylthio group in erucin is hydrophobic (miLog$P = 0.84$), whereas the methylsulfinyl group in sulforaphane is relatively hydrophilic (miLog$P = -0.69$). Previous studies have indicated that the hydrophobicity of a carrier plays a crucial role in protein binding stability [43]. As shown in Fig. S7 (Supporting information), while Gru88 can efficiently form uniform nanoparticles around 500 nm with GFP in aqueous solution, the Gsfn86/GFP complex is relatively loose, with an average particle size exceeding 1000 nm.

We then investigated the protein binding affinity of the synthesized polymers using a fluorescence quenching assay. As shown in Figs. 2k–m, both Gru88 and Gsfn86 significantly reduced the FI of GFP upon complexation in aqueous solution. In the presence of 110 mmol/L NaCl, the FI of the Gsfn86/GFP complex solution was completely recovered due to weakened ionic interactions between Gsfn86 and GFP. In contrast, the Gru88/GFP complexes, which are formed through both hydrophobic and ionic interactions, exhibited relatively stable nanoparticles in the presence of NaCl, and the FI of the Gru88/GFP complex solution was only partially recovered. Sodium dodecyl sulfate-polyacrylamide gel electrophoresis (SDS-PAGE) analysis also confirmed this result (Fig. S8 in Supporting information). We further investigated the stability of the complex under cell culture conditions using RBITC-labeled polymers. As shown in Figs. 2n and o, after adding the RBITC-Gru88/GFP complex to the 143B cells, the material and protein formed a yellow fluorescent complex, accumulating on the cell surface and facilitating subsequent cell uptake. In contrast, neither green nor red fluorescence signals were detected around the cells after the addition of the RBITC-Gsfn86/GFP complex, indicating that the complex had dissociated in the culture medium. Taken together, these results suggested that the structural difference between sulforaphane and erucin, specifically the hydrophobic methylthio group in erucin and the hydrophilic methylsulfinyl group in sulforaphane, significantly impacts their performance in protein delivery.

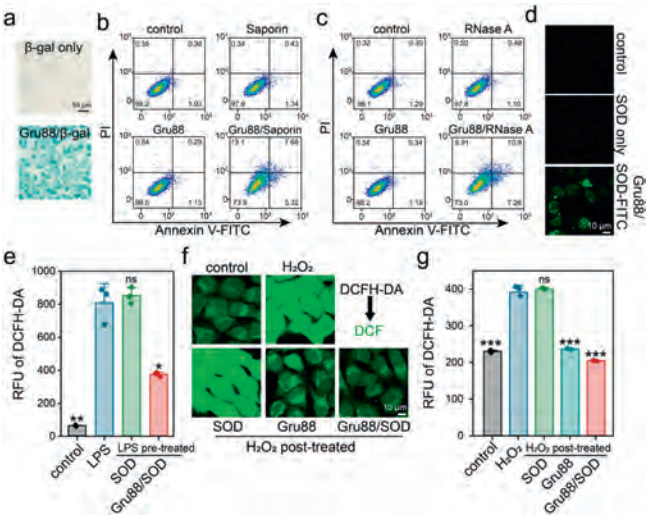


Fig. 3. Intracellular delivery of bioactive enzymes. (a) Cytosolic delivery of β-Gal by Gru88 in 143B cells, determined by X-gal staining. (b) Apoptosis ratio of 143B cells treated with saporin, Gru88, and Gru88/saporin complexes. The concentration of saporin and Gru88 were 0.01 and 25 μg/mL, respectively. (c) Apoptosis ratio of 143B cells treated with RNase A, Gru88, and Gru88/RNase A complexes. The concentration of RNase A and Gru88 were 0.5 and 25 μg/mL, respectively. (d) Confocal images of 143B cells treated with Gru88/SOD-FITC for 0.5 h. (e) FI of ROS in RAW264.7 cells. RAW264.7 cells were pretreated with LPS (1 μg/mL) for 12 h, followed by incubation with the Gru88/SOD complexes for 0.5 h. Confocal images (f) and FI (g) of ROS in 143B cells. The cells were pretreated with Gru88/SOD for 0.5 h, followed by incubation with H_2O_2 (500 μmol/L) for 0.5 h. The concentrations of Gru88 and SOD were 25 and 40 μg/mL, respectively. Data are presented as mean ± s.d. ($n = 3$). $^{ns}P > 0.05$, $^{*}P < 0.05$, $^{**}P < 0.01$, $^{***}P < 0.001$.

Rapid delivery of proteins into the cytoplasm is essential for preserving their biological functions. To assess the efficacy of Gru88 in delivering bioactive enzymes, we first tested its ability to deliver β-galactosidase (β-gal), an enzyme that specifically hydrolyzes β-galactosidic bonds. As shown in Fig. 3a, Gru88 successfully delivered the enzyme into 143B cells within 30 min, where it catalyzed the hydrolysis of the colorless substrate 5–bromo-4–chloro-3-indolyl-β-D-galactoside (X-Gal), producing an insoluble blue precipitate.

Saporin, a ribosome-inactivating protein with potent anticancer properties, and RNase A, which degrades intracellular RNAs and induces toxicity upon delivery, were also evaluated. As demonstrated in Fig. 3b, Gru88 efficiently delivered the membrane-impermeable saporin into 143B cells, inducing significant apoptosis. In contrast, free saporin or Gru88 alone induced minimal toxicity. Similarly, substantial apoptosis was observed in 143B cells treated with the Gru88/RNase A complex, whereas neither Gru88 nor RNase A alone caused noticeable toxicity (Fig. 3c).

Next, we tested the ability of Gru88 to deliver the antioxidant enzyme SOD. To visualize intracellular delivery, SOD was labeled with fluorescein isothiocyanate (FITC). As shown in Fig. 3d, Gru88 efficiently delivered the membrane-impermeable SOD-FITC into 143B cells within 30 min. In addition, as shown in Fig. S9 (Supporting information), the activity of SOD has been well-preserved during the delivery process. We then evaluated the ability of the

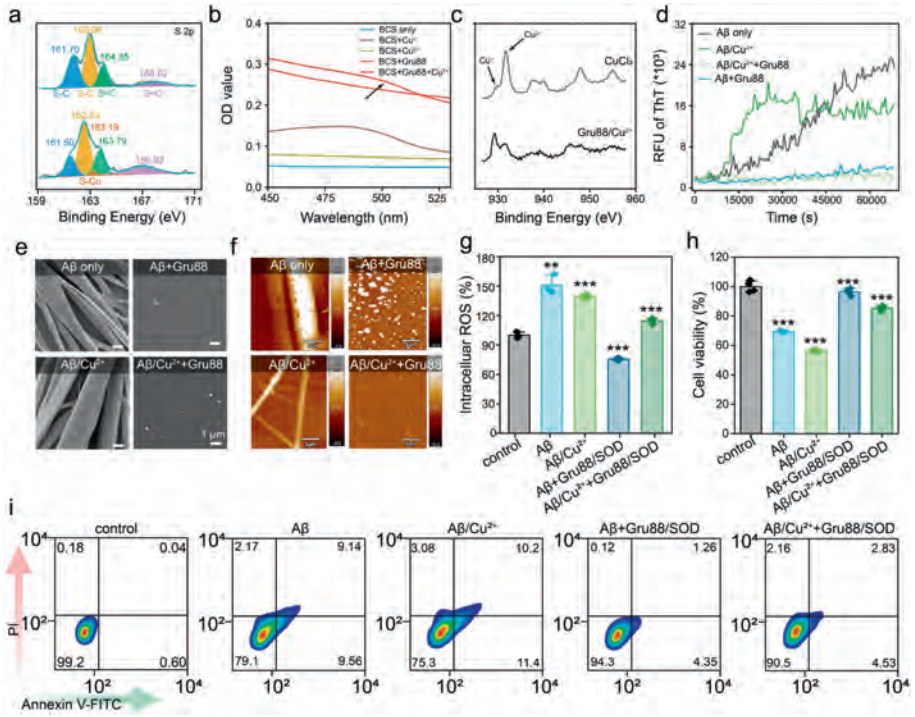


Fig. 4. Inhibition effect of Gru88 on Aβ amyloidosis. (a) Characterization of Cu^{2+} coordinated Gru88 by XPS. (b) Ultraviolet-visible (UV–vis) spectrum of various materials incubated with BCS. (c) XPS of free Cu^{2+} ion and Gru88/Cu^{2+}. (d) ThT fluorescence assay for amyloid fibril detection of Aβ and Aβ/Cu^{2+} system in the absence and presence of Gru88. Scanning electron microscope (SEM, e) and atomic force microscope (AFM, f) examination of the formed amyloid fibril under various conditions. The doses of ThT, Aβ, Gru88 and Cu^{2+} were 20, 30, 0.2 and 30 μmol/L, respectively. (g) ROS levels of PC12 cells treated with Aβ or Aβ/Cu^{2+} for 2 h in the absence and presence of Gru88/SOD. (h) Cell viability of PC12 cells treated with Aβ or Aβ/Cu^{2+} for 24 h in the absence and presence of Gru88/SOD. (i) Apoptosis ratio of PC12 cells treated with Aβ or Aβ/Cu^{2+} for 12 h in the absence and presence of Gru88/SOD. The doses of Aβ, Cu^{2+}, SOD and Gru were 30 μmol/L, 30 μmol/L, 25 μg/mL and 10 μg/mL, respectively.

Gru88/SOD complex to regulate intracellular ROS levels in two separate experiments. First, Gru88/SOD treatment significantly reduced intracellular ROS levels induced by lipopolysaccharide (LPS) stimulation in RAW264.7 macrophages (Fig. 3e). Second, 143B cells pre-incubated with Gru88/SOD complexes exhibited a marked reduction in ROS levels triggered by H_2O_2 exposure (Figs. 3f and g). Specifically, Gru88 functions as a hydrogen peroxide (H_2O_2)-decomposing mimic of endogenous catalase, effectively scavenging ROS such as H_2O_2 (Fig. S10 in Supporting information). We then conducted *in vitro* experiments using LPS-stimulated macrophages (RAW264.7 cells) as a model of inflammation. As shown in Fig. S11 (Supporting information), Gru88/SOD significantly reduced the secretion of pro-inflammatory cytokines TNF-α and IL-6 compared to untreated LPS-activated cells. Importantly, this anti-inflammatory effect was observed even for Gru88 alone (without SOD cargo), suggesting that the polysulfide-driven ROS-scavenging mechanism synergizes with its cargo-delivery function to attenuate inflammation. These findings suggest that the Gru88 complex can efficiently deliver SOD into cells, helping to maintain ROS homeostasis in healthy cells and reduce ROS levels and inflammation levels in inflammatory cells.

Thiourea and thioether groups are widely recognized for their remarkable ability to coordinate with copper ions. Drawing on this knowledge, we postulate that the abundant thiourea and thioether groups in Gru88 confer potent copper ion binding capabilities. These capabilities hold promise for alleviating pathological conditions associated with copper ion imbalance through chelation. To test this hypothesis, we utilized X-ray photoelectron spectroscopy (XPS) to scrutinize the coordination of copper ions with Gru88. As shown in Fig. 4a, in the case of Gru88, the S 2p peaks at 161.70 and 163.08 eV were ascribed to the –C–S moiety, while the peak at 164.35 eV corresponded to –C=S. A peak at 168.62 eV, assignable to –S=O, was also detected, presumably resulting from the oxidation of thiourea or thioether [44–46]. Upon coordination with Cu^{2+} ions, all of these peaks exhibited a slight shift towards lower binding energies. Moreover, after coordination with Cu^{2+}, a new peak emerged at 163.19 eV, which was attributed to the Cu-S bond. Notably, the N 1s peaks of Gru88 showed only minor shifts after coordination (Fig. S12 in Supporting information) [47]. These findings clearly indicate that copper ions predominantly coordinate with the sulfur atom rather than the nitrogen atom in the polymer. Previous reports have indicated that the coordination of thiourea with copper ions results in the reduction of Cu^{2+} to Cu^{+} [48–50]. To delve deeper into this phenomenon, we employed the well-established bathocuproine disulfonate (BCS) assay to examine the Gru88/Cu^{2+} coordination polymer. BCS has a high selectivity for coordinating with Cu^{+} ions, forming a BCS-Cu^{+} complex that exhibits a characteristic absorption peak at approximately 485 nm. As illustrated in Fig. 4b, when BCS was added to the Gru88/Cu^{2+} system, an absorption peak emerged. In contrast, no such peak was detected when BCS was added to either Cu^{2+} alone or Gru88 alone. This observation strongly suggests that a portion of the Cu^{2+} ions in the Gru88/Cu^{2+} complex is reduced to Cu^{+}. The reduction of Cu^{2+} to Cu^{+} was further confirmed by XPS (Fig. 4c), which showed that some copper ions in the Gru88/Cu^{2+} complex are indeed in the Cu^{+} state.

Both APP and Aβ peptides contain copper-binding sites. Research has shown that their interaction with Cu^{2+} ions can trigger the production of ROS, particularly highly reactive hydroxyl radicals. These free radicals can cause oxidative damage to Aβ peptides and nearby molecules, such as proteins and lipids, ultimately leading to neurotoxic effects [37]. To further investigate the potential of Gru88, we examined its ability to inhibit copper-mediated Aβ peptide amyloidosis. Thioflavin T (ThT), a widely used benzothiazole dye, is commonly employed to detect and quantify amyloid fibrils and aggregates [51]. When ThT binds to amyloid fibrils, its

fluorescence is enhanced at 485 nm. As shown in Fig. 4d, the FI of ThT steadily increased over the times, indicating the onset of Aβ fibrillization. The presence of Cu^{2+} ions significantly accelerated this process, suggesting that abnormal metal regulation can lead to faster fibrillization of amyloid proteins. Interestingly, the addition of a small amount of Gru88 effectively prevented Aβ fibrillization, regardless of the presence of Cu^{2+} ions. Throughout the entire incubation period, fluorescence values remained low, indicating inhibition of fibril formation. Microscopic analysis revealed that the original Aβ fibrils had smooth surfaces and were primarily long, strip-like structures, either individual or in clusters. These fibrils could reach widths of several micrometers and lengths of several tens of micrometers (Figs. 4e and f). However, when Aβ was incubated with Gru88, regardless of the presence or absence of copper ions, it predominantly maintained a spherical shape, with only occasional short, block-like aggregates and no obvious fibrils formed. Taken together, these findings clearly demonstrate that Gru88 can effectively inhibit the aggregation of Aβ peptides, irrespective of the involvement of metal ions.

Finally, we used PC12 cells as a neuronal model to further investigate the neuroprotective mechanism of Gru88 by intracellularly delivering SOD [52]. As shown in Figs. 4g-i, both fibrillized Aβ and Aβ/Cu^{2+} triggered the production of ROS in PC12 cells, leading to a higher incidence of apoptosis and reduced cell survival rates. In contrast, treatment with Gru88/SOD significantly downregulated the intracellular ROS levels, enhanced cell viability, and reduced the rate of apoptosis.

In summary, we have successfully engineered a multifunctional protein delivery system by incorporating erucin onto cationic polymers. The representative polymer Gru88 can rapidly transport target proteins into cells *via* a membrane perforation mechanism. This rapid delivery approach effectively preserves the activity of the target proteins. The incorporation of erucin introduces a substantial number of thiourea and thioether groups into the polymer carrier. These groups endow the material with exceptional copper ion binding capabilities, which can be harnessed to ameliorate the pathological environment associated with copper homeostasis imbalance. Gru88 is highly effective in inhibiting the fibrillar aggregation of Aβ peptides, whether mediated by copper ions or independent of them. Moreover, by delivering the antioxidant enzyme SOD, Gru88 effectively suppresses the intracellular ROS levels induced by the fibrillar aggregation of Aβ peptides. Consequently, it reduces the apoptosis rate, demonstrating its potential in mitigating the detrimental effects associated with Aβ peptide aggregation. For future *in vivo* studies, we propose functionalizing the nanoparticles with blood-brain barrier-targeting ligands, such as transferrin receptor antibodies or angiopep-2 peptides, which exploit receptor-mediated transcytosis.

Declaration of competing interest

The authors declare that they have no known competing financial interests or personal relationships that could have appeared to influence the work reported in this paper.

CRediT authorship contribution statement

Le Chen: Writing – original draft, Methodology, Investigation, Data curation. **Hui Wang:** Writing – review & editing, Writing – original draft, Supervision, Project administration, Conceptualization. **Yiyun Cheng:** Writing – review & editing, Visualization, Supervision, Project administration, Funding acquisition, Conceptualization.

Acknowledgments

The authors thank the supports from the National Key R&D Program of China (No. 2024YFA1210100), the National Natural Science Foundation of China (No. 22135002), and East China Normal University Multifunctional Platform for Innovation (004).

Supplementary materials

Supplementary material associated with this article can be found, in the online version, at doi:10.1016/j.cclet.2025.111172.

References

[1] P. Scheltens, B. De Strooper, M. Kivipelto, et al., Lancet 397 (2021) 1577–1590.
[2] J. Gu, J. Gu, L. Yu, Chin. Chem. Lett. 36 (2025) 110727.
[3] J.A. Hardy, G.A. Higgins, Science 256 (1992) 184–185.
[4] J. McDaid, S. Mustaly-Kalimi, G.E. Stutzmann, Cells 9 (2020) 2655.
[5] M. Calvo-Rodriguez, B.J. Bacskai, Trends Neurosci. 44 (2021) 136–151.
[6] A.Y. Baev, A.Y. Vinokurov, I.N. Novikova, et al., Cells 11 (2022) 706.
[7] Q. Hongshuang, W. Jiasi, R. Jinsong, et al., CCS Chem. 1 (2019) 313–325.
[8] F. Shehjar, D.A. Almarghalani, R. Mahajan, et al., Cells 13 (2024) 188.
[9] C. Oh, T. Nakamura, X. Zhang, S.A. Lipton, Neuron 112 (2024) 3823–3850.
[10] J.M. Tarasoff-Conway, R.O. Carare, R.S. Osorio, et al., Nat. Rev. Neurol. 11 (2015) 457–470.
[11] Z. Yu, J. Yu, C. Jingshan, et al., CCS Chem. 3 (2020) 2316–2330.
[12] Q. Feng, X. Zhang, N. Zhang, et al., Exploration 4 (2024) 20230048.
[13] J.W. Karr, L.J. Kaupp, V.A. Szalai, J. Am. Chem. Soc. 126 (2004) 13534–13538.
[14] C. Hureau, Chem. Rev. 256 (2012) 2164–2174.
[15] A.I. Bush, W.H. Pettingell, G. Multhaup, et al., Science 265 (1994) 1464–1467.
[16] C.F. Zhang, L. Fan, P. Yang, Chin. Chem. Lett. 18 (2007) 97–98.
[17] W. Li, M.J. Dong, H. Dai, et al., Chin. Chem. Lett. 36 (2025) 110614.
[18] C. Xie, J. Liao, Y. Li, et al., Chin. Chem. Lett. 37 (2026) 110956.
[19] K. Reybier, S. Ayala, B. Alies, et al., Angew. Chem. Int. Ed. 55 (2016) 1085–1089.
[20] J. Yoo, J. Lee, B. Ahn, et al., Chem. Sci. 16 (2025) 2105–2135.
[21] H. Fanlo-Ucar, P. Picón-Pagès, V. Herrera-Fernández, et al., Antioxidants 13 (2024) 1208.
[22] Q. Zhang, Y. Li, Q. Jin, Chin. Chem. Lett. 37 (2026) 110964.
[23] A. Martelli, E. Piragine, E. Gorica, et al., Antioxidants 10 (2021) 961.
[24] M. Shimoyama, Y. Hosokawa, I. Hosokawa, K. Ozaki, et al., Immunopharmacol. Immunotoxicol. 46 (2024) 49–54.
[25] C. Li, S. Song, Y. He, et al., Food Res. Int. 150 (2021) 110807.
[26] D. Grami, S. Selmi, K. Rtibi, et al., Nutrients 16 (2024) 253.
[27] S. Han, J. Wu, ACS Appl. Mater. Interfaces 14 (2022) 55944–55956.
[28] S. Han, P. Xin, Q. Guo, et al., Adv. Healthc. Mater. 12 (2023) 4060.
[29] H. Zhao, Z.Y. Lin, L. Yildirimer, et al., J. Mater. Chem. B 4 (2016) 4060–4071.
[30] L. Jin, J. Zhang, L. Nie, et al., Chin. Chem. Lett. 36 (2025) 110774.
[31] S. Chowdhury, I. Toth, R.J. Stephenson, Biomaterials 280 (2022) 121303.
[32] D.A. Tomalia, L.A. Reyna, S. Svenson, Biochem. Soc. Trans. 35 (2007) 61–67.
[33] Z. Zhe, G. Xin, L. Yanwen, et al., CCS Chem. 5 (2022) 1411–1421.
[34] C. Wenhua, C. Kunyu, G. Yunqing, et al., CCS Chem. 7 (2025) 2394–2408.
[35] L. Kong, S.H.C. Askes, S. Bonnet, et al., Angew. Chem. Int. Ed. 55 (2016) 1396–1400.
[36] P. Guo, D. Liu, K. Subramanyam, et al., Nat. Commun. 9 (2018) 130.
[37] A. Moscho, O. Orwar, D.T. Chiu, et al., Proc. Natl. Acad. Sci. U. S. A. 93 (1996) 11443–11447.
[38] M. Liang, Q. Wang, S. Zhang, et al., Adv. Mater. 36 (2024) 2409015.
[39] J. Van Hoeck, T. Van de Vyver, A. Harizaj, et al., Adv. Mater. 33 (2021) 2008054.
[40] S. Wang, R. Chen, Chem. Mater. 29 (2017) 5806–5815.
[41] C. Chestnut, D. Subramaniam, P. Dandawate, et al., Nutr. Cancer 73 (2021) 2249–2271.
[42] Y. Zhang, P. Talalay, C.G. Cho, et al., Proc. Natl. Acad. Sci. U. S. A. 89 (1992) 2399–2403.
[43] Z. Chen, Z. Wei, F. Xiao, et al., Adv. Funct. Mater. 32 (2022) 2207845.
[44] C. Xu, Y. Xu, D. Zhong, et al., Carbohydr. Polym. 296 (2022) 119872.
[45] I.M. Germaine, M.B. Huttel, M.P. Alderman, et al., ACS Appl. Mater. Interfaces 15 (2023) 37764–37774.
[46] Z. Luo, S. Chenxing, T. Yizheng, CCS Chem. 4 (2021) 2239–2248.
[47] Z. Anfar, A. Amedlous, M. Majdoub, et al., RSC Adv. 10 (2020) 31087–31100.
[48] S. Shao, Q. Zhou, J. Si, et al., Nat. Biomed. Eng. 1 (2017) 745–757.
[49] M. Liang, Y. Cheng, H. Wang, Chem. Eur. J. 29 (2023) e202300131.
[50] B. Halliwell, J. Neurochem. 97 (2006) 1634–1658.
[51] A. Chauhan, V.P.S. Chauhan, R. Rubenstein, et al., Neurochem. Res. 22 (1997) 227–232.
[52] M.A. Dichter, A.S. Tischler, L.A. Greene, Nature 268 (1977) 501–504.